Harmonically Trapped Atoms with Spin-Orbit Coupling

Chuanzhou Zhu[1], Lin Dong[1], and Han Pu[1,2]

[1]*Department of Physics and Astronomy, and Rice Center for Quantum Materials, Rice University, Houston, TX 77251, USA*
[2]*Center for Cold Atom Physics, Chinese Academy of Sciences, Wuhan 430071, P. R. China*
(Dated: January 8, 2016)

We study harmonically trapped atoms subjected to an equal combination of Rashba and Dresselhaus spin-orbit coupling induced by Raman transition. We first examine the wave function and the degeneracy of the single-particle ground state, followed by a study of two weakly interacting bosons or fermions. For the two-particle ground state, we focus on the effects of the interaction on the degeneracy, the spin density profiles, and the density-density correlation functions. Finally we show how these studies help us to understand the many-body properties of the system.

I. INTRODUCTION

In recent years, spin-orbit coupling and synthetic gauge fields [1, 2] in ultracold atomic gases have attracted a great amount of interest. With equal Rashba and Dresselhaus strengths, spin-orbit coupling in both atomic Bose [3–5] and Fermi [6, 7] gases have been realized in experiments. Theoretically, it was predicted that such systems would exhibit novel quantum phases for both bosonic [8, 9] and fermionic [10, 11] cases, as well as unique features such as the stripe pattern in many-body density profile [8, 12, 13]. For spin-orbit coupled systems in uniform space, the single-particle ground state [14] can be easily obtained, and the ground states of two-body [15, 16] and many-body [12] systems with zero-range contact interactions have been analytically calculated by scattering theory and mean field approaches, respectively. Compared with investigating these systems in uniform space, it may be more relevant and realistic to consider the systems in a harmonic trap, as a trapping potential is always present in cold atom experiment. The energy spectra of trapped single-particle [16–18] and two-particle [19, 20] systems with spin-orbit coupling have been numerically studied. However, a systematic investigation of the single-particle and two-particle ground states, and how they are related to the many-body physics of the trapped system is still lacking.

In this paper we aim to present such a study. We systematically investigate the ground states of a single particle, two bosons, and two fermions confined in a one-dimensional (1D) harmonic trap with Raman-induced spin-orbit coupling. For the single-particle ground state, which is presented in Sec. II, we obtain the wave functions through imaginary time evolution and demonstrate how the Raman coupling strength and the trap frequency affect the degeneracy. In Sec. III we consider two weakly interacting bosons. The degeneracy, the entanglement, the density-density correlation functions, and the spin density profiles of the ground state are studied by varying the spin-dependent contact interaction, the Raman coupling strength, and the two-photon detuning. Our

results demonstrate that the spin-dependent interaction breaks the ground state degeneracy of this system, and also imprints a stripe pattern in the density-density correlation. We propose an experimental scheme to measure the energy gap between the ground state and the first excited state of the system through a resonance excitation process [22, 23] in Sec. V. In addition, the connection between the behaviors of two-boson and many-boson ground states are discussed. To investigate the effect of quantum statistics, we then consider a system of two fermions in Sec. IV and show how they differ from the system of two bosons. Finally, we conclude in Sec. VI.

II. SINGLE-PARTICLE GROUND STATE

In this section, we consider a single spin-$1/2$ atom confined in a 1D harmonic trap with frequency ω, subjected to the Raman-induced spin-orbit coupling, with two-photon recoil momentum q_r, Raman coupling strength Ω, and two-photon detuning δ. The Hamiltonian then takes the form

$$h = \frac{\hat{p}^2}{2m} + \frac{1}{2}m\omega^2 x^2 + \frac{q_r\hat{p}}{m}\sigma_z + \frac{\Omega}{2}\sigma_x + \frac{\delta}{2}\sigma_z, \quad (1)$$

where σ_x and σ_z denote the x and z components of Pauli matrices, m is the atomic mass, $\hat{p} = -i\hbar\partial/\partial x$ is the momentum operator, and x is the position. The two spin states are defined as $\sigma_z|\uparrow\rangle = |\uparrow\rangle$ and $\sigma_z|\downarrow\rangle = -|\downarrow\rangle$, respectively. We mainly consider the case with $\delta = 0$, and the influence of finite δ will be briefly discussed.

A. Homogeneous system

We first briefly review the case when there is no trap [14], i.e., $\omega = 0$. For this case, the system possesses translational symmetry and thus the momentum p is a good quantum number. When $\delta = 0$, the single-particle dispersion is given by

$$\epsilon_p = \frac{p^2}{2m} \pm \sqrt{\frac{q_r^2 p^2}{m^2} + \frac{\Omega^2}{4}}. \quad (2)$$

For $\Omega < 4E_r$ (where $E_r \equiv q_r^2/(2m)$ is the recoil energy), ϵ_p displays two degenerate minima at $p = \pm k \equiv \pm q_r \sqrt{1 - (\Omega/4E_r)^2}$, corresponding to two orthogonal degenerate ground states

$$\langle x\sigma | g_1 \rangle = e^{ikx} \left[\cos\theta_k \quad -\sin\theta_k \right]^T , \tag{3}$$

$$\langle x\sigma | g_2 \rangle = e^{-ikx} \left[\sin\theta_k \quad -\cos\theta_k \right]^T , \tag{4}$$

where $\sigma = \uparrow (\downarrow)$ marks the spin up (down) state, and $\tan\theta_k = \frac{2}{\Omega} \left(\frac{q_r k}{m} + \sqrt{\frac{q_r^2 k^2}{m^2} + \frac{\Omega^2}{4}} \right)$. For $\Omega > 4E_r$, the single particle dispersion has only a single minimum at $p = 0$ and the non-degenerate ground state takes the form

$$\langle x\sigma | g \rangle = \left[1/\sqrt{2} \quad -1/\sqrt{2} \right]^T . \tag{5}$$

B. Trapped system

The presence of a harmonic trap breaks the translational symmetry of the system, and we have to resort to numerical calculations to study the properties of the ground state. Using the finite difference method to discretize $\hat{p}$ and x, we obtain eigenenergies through the diagonalization of the single-particle Hamiltonian (1), and the ground-state wave function by imaginary time evolution. At $\delta = 0$, Hamiltonian (1) possesses the following symmetry: If $|\psi\rangle$ is an eigenstate of h, $|\psi'\rangle = \sigma_x K |\psi\rangle$, where K represents complex conjugate operator, is also an eigenstate with the same eigenenergy. However, unlike the time reversal symmetry of a spin-1/2 system which results in Kramer degeneracy, the current symmetry does not guarantee degenerate eigenstates. For a non-degenerate state $|\psi\rangle$, the above symmetry property necessarily requires $|\psi'\rangle = \sigma_x K |\psi\rangle$ to differ from $|\psi\rangle$ by at most a overall phase factor. In Fig. 1(a) we exhibit low-lying energy spectrum for a trapped system with three different values of Raman coupling strength Ω. Each red (blue) dot represents the energy of a two-fold degenerate (non-degenerate) eigenstate. At $\Omega = 0$, we have two uncoupled spin states, and all the single-particle states must be trivially two-fold degenerate. As Ω increases, degeneracies of the high-energy states start to be lifted first. Eventually, at a critical coupling strength Ω_c, degeneracy of the ground state is also lifted and all the single particle eigenstates become non-degenerate. The energy difference $\Delta\epsilon$ between the two lowest-lying states is shown in Fig. 1, as a function of Ω for various trap frequencies ω. For a fixed value of the trap frequency ω, with increasing Ω, $\Delta\epsilon$ changes from zero to finite when Ω exceeds Ω_c, signaling that the ground state changes from being two-fold degenerate to non-degenerate. The critical value Ω_c at which the ground state degeneracy is lifted is a decreasing function of the trap frequency ω, and in the limit $\omega \to 0$, $\Omega_c = 4E_r$ and we recover the result for the homogeneous system.

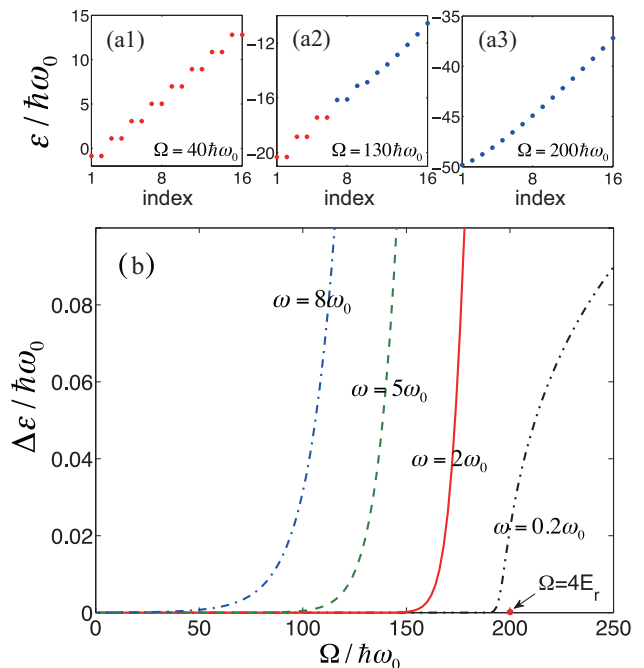FIG. 1: (color online) (a_1)-(a_3) The first 16 single-particle eigenenergies with trap frequency $\omega = 2\omega_0$ for several different values of Raman coupling strength $\Omega/(\hbar\omega_0) = 40, 130, 200$. Red dots correspond to two-fold degenerate eigenstates and blue dots correspond to non-degenerate eigenstates. (b) Energy gap $\Delta\epsilon$ between the two lowest energy eigenstates as a function of Ω for different values of trap frequency. Other parameters used are: the recoil momentum $q_r = 10\sqrt{m\hbar\omega_0}$ and two-photon detuning $\delta = 0$. Throughout this paper, we choose $\omega_0 = 2\pi \times 10^2$Hz to be the units for frequency and take m to be the mass of the ^{87}Rb atom.

The degeneracy breaking of single-particle eigenstates at large Ω can be intuitively understood as follows. The Raman coupling term, $\Omega\sigma_x/2$, in Hamiltonian (1) behaves like an effective Zeeman field in x-direction. At large Ω, this effective Zeeman field is so strong that it polarizes the spin-1/2 particle by aligning its spin along the x-axis, and the particle essentially becomes a scalar particle as its spin degrees of freedom is frozen. It is a well known fact that, for a scalar particle, there is no degenerate bound state in 1D [21].

The two-component spinor wave function of a single particle can be written as $\left[\phi_\uparrow(x) \quad \phi_\downarrow(x) \right]^T$, where $\phi_\sigma(x) = |\phi_\sigma(x)| e^{i\theta_\sigma(x)}$ is in general complex with phase angle $\theta_\sigma(x)$. In Fig. 2, we exhibit the ground state wave function for $\omega = 2\omega_0$ (which corresponds to the red solid line in Fig. 1(b)) and two different values of Ω.

When $\Omega = 130\hbar\omega_0$, the ground states are two-fold degenerate, and the two degenerate states are transformed to each other by the symmetry operation $\sigma_x K$. The spin density profiles for the two degenerate ground states are depicted in Fig. 2(a) and (c), with the corresponding phase angles plotted in Fig. 2(b) and (d), respec-
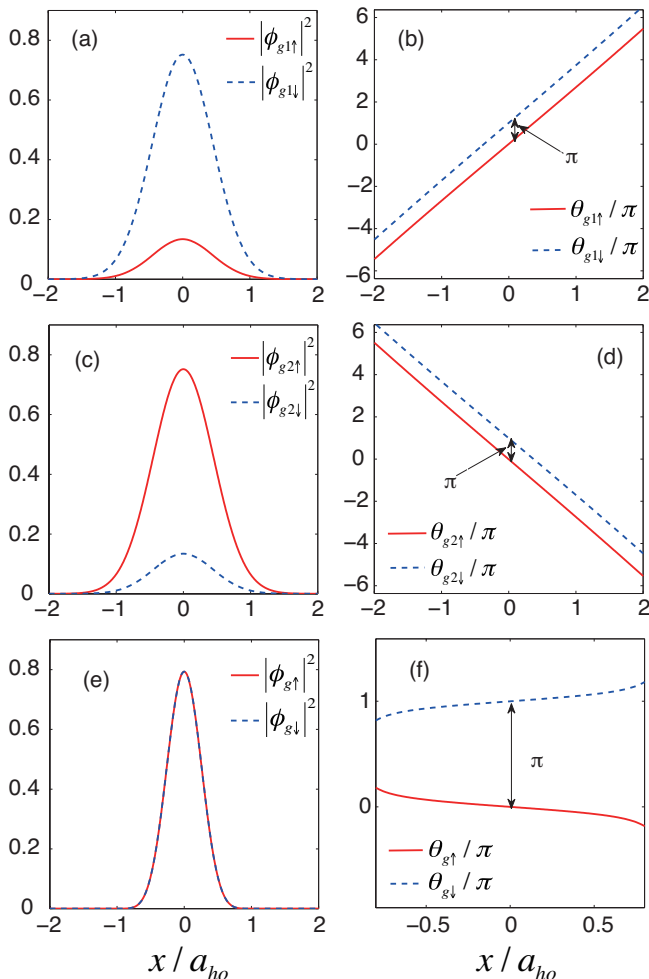
FIG. 2: (color online) Single-particle ground state wave functions with $\omega = 2\omega_0$, $q_r = 10\sqrt{m\hbar\omega_0}$, and $\delta = 0$. Red solid line and blue dashed line correspond to the spin-up component and the spin-down component, respectively. For two degenerate ground states at $\Omega = 130\hbar\omega_0$, (a)(c) are the real space probability profiles, and (b)(d) are the phase angles. For the non-degenerate ground state at $\Omega = 200\hbar\omega_0$, (e) is the real space probability profile, and (f) is the phase angle. We define $a_{ho} = \sqrt{\frac{\hbar}{m\omega_0}}$.

tively. These plots suggest that we can approximately write down the ground state wave functions as

$$\langle x\sigma | g_1 \rangle = e^{ikx} \left[\ \phi_1(x)\ -\phi_2(x)\ \right]^T , \qquad (6)$$

$$\langle x\sigma | g_2 \rangle = e^{-ikx} \left[\ \phi_2(x)\ -\phi_1(x)\ \right]^T , \qquad (7)$$

where $\phi_{1(2)}(x)$ is real and $\left[\phi_{1(2)}(x)\right]^2$ is represented by the red solid (blue dashed) line in Fig. 2(a), and k is the slope of the phase angles in Fig. 2(b). The density profiles of both $|g_1\rangle$ and $|g_2\rangle$ depicted in Fig. 2(a) and (c) are smooth in real space. These two states can be regarded as the analogies of the degenerate ground states for the uniform system, see Eqs. (3) and (4). However, due to the degeneracy, any linear superposition of $|g_1\rangle$

and $|g_2\rangle$ represents a ground state of the system. Such superposition state will exhibit stripe pattern in its real space probability profile.

When $\Omega = 200\hbar\omega_0$, the ground state is non-degenerate. This state is depicted in Fig. 2(e) and (f). The symmetry property under the operation $\sigma_x K$ guarantees that, for a non-degenerate state, we must have $|\phi_\uparrow(x)| = |\phi_\downarrow(x)|$ and $\theta_\uparrow(x) + \theta_\downarrow(x) =$ const. As can be seen from Fig. 2(e) and (f), these conditions are indeed satisfied by the non-degenerate ground state. Furthermore, the phase angles are almost uniform. As a result, this ground state can be approximately represented by

$$\langle x\sigma | g \rangle = \phi_0(x) \left[1/\sqrt{2} \quad -1/\sqrt{2}\right]^T , \qquad (8)$$

where $\phi_0(x)$ is a real function and $\left[\phi_0(x)\right]^2/2$ is plotted in Fig. 2(e). This state is obviously the analogy of the non-degenerate ground state for the uniform system represented by Eq. (5).

Now we briefly discuss the case with finite δ. In this case, the single-particle state is always non-degenerate, possessing a non-vanishing magnetization $\langle \sigma_z \rangle$. In addition, the real-space wave packet of the ground state is always smooth.

III. TWO-BOSON GROUND STATE

The two-body physics of trapped particles with spin-orbit coupling has some non-trivial features. The research by D. Blume's group has investigated how the real-space spin structure [19] and the eigenenergy spectrum [20] depend on q_r, Ω, and the interaction strength (In those works, the interaction has SU(2) symmetry, i.e., the interaction between different spins are characterized by the same interaction strength). Here we investigate the system from a different perspective and focus on different parameter regimes. We study degeneracies, density-density correlations, and density profiles of the ground states, investigate connections between single-particle, two-particle, and many-particle ground states, and consider the parameters from current ^{87}Rb experiments with a spin-dependent interaction.

In this section, we consider two weakly interacting spin-orbit coupled bosons in a harmonic trap. To this end, we use the single-particle eigenstates discussed in the previous section to construct a set of two-body symmetric basis vectors for expanding two-boson Hamiltonian. We label the single-particle eigenstates $|i\rangle$ with corresponding eigenenergies ϵ_i. Then states $|ii\rangle_b \equiv |i\rangle_1 |i\rangle_2$, and $|ij\rangle_b \equiv \frac{1}{\sqrt{2}} (|i\rangle_1 |j\rangle_2 + |j\rangle_1 |i\rangle_2)$ for $i > j$ form the symmetric two-particle basis. Here $1, 2$ are particle indices and we take a cut-off for i, j in numerical calculation. Then the matrix elements of two-particle Hamiltonian

$$H = h_1 + h_2 + \hat{V} , \qquad (9)$$

with h_1 and h_2 being the single particle Hamiltonian and $\hat{V}$ the two-body contact interaction potential, can be written as

$$\langle ij| (h_1 + h_2) |kl\rangle_b = (\epsilon_i + \epsilon_j)\, \delta_{ik}\delta_{jl}\,, \qquad (10)$$

and

$$\langle ij| \hat{V} |kl\rangle_b = \sum_{\sigma_1\sigma_2} g_{\sigma_1\sigma_2} \int dx\, f^{ij}_{\sigma_1\sigma_2}(x) \left[f^{kl}_{\sigma_1\sigma_2}(x)\right]^*\,, \quad (11)$$

with $f^{ij}_{\sigma_1\sigma_2}(x) =_b \langle ij| x\sigma_1\rangle_1 |x\sigma_2\rangle_2$. Away from the confinement induced resonance, the quasi-1D interaction strength $g_{\sigma_1\sigma_2}$ is related to the 3D interaction strength $g_{3D\sigma_1\sigma_2}$ as $g_{\sigma_1\sigma_2} = \frac{m\omega_\perp}{2\pi\hbar} g_{3D\sigma_1\sigma_2}$, where $\omega_\perp$ is the strong transverse trap frequency. In this paper we assume a spin symmetric interaction with $g_{\uparrow\uparrow} = g_{\downarrow\downarrow} \equiv g$. In our calculation, we take $g_{3D\uparrow\uparrow} = g_{3D\downarrow\downarrow} = 7.79 \times 10^{-12}$Hz cm^3, which is from current experiments in ^{87}Rb [14]. In the scope of this paper, this interaction is relatively weak compared with center-of-mass motion energy and the spin-orbit-coupling energy, and hence the ground state of two interacting particles will not deviate much from the ground state in the non-interacting case. To characterize the properties of the ground state, we investigate the density-density correlation function which is defined as

$$C^b_{\sigma_1\sigma_2}(x_1, x_2) \equiv \langle\Psi_g| \hat{n}_{\sigma_1}(x_1) \hat{n}_{\sigma_2}(x_2) |\Psi_g\rangle$$
$$= 2 \left|_1\langle x_1\sigma_1|_2 \langle x_2\sigma_2| \Psi_g\rangle\right|^2\,, \qquad (12)$$

and the density profile which is defined as

$$n^b_\sigma(x) \equiv \langle\Psi_g| \hat{n}_\sigma(x) |\Psi_g\rangle\,, \qquad (13)$$

where $\hat{n}_\sigma(x)$ is the density operator of spin σ and $|\Psi_g\rangle$ represents the two-boson ground state in this section.

A. Two-body phase diagram at $g_{\uparrow\downarrow} = 0.6g$

We obtain the low-lying eigenstates of the two-boson system by diagonalizing H after it is expanded onto the symmetric two-particle basis states $|ij\rangle_b$. Here we still consider the case with $\delta = 0$. From the previous study of many-boson physics, we know that the stripe phase only appears with small δ, so this regime contains the most abundant many-boson physics. In Fig. 3(a), we plot the energies of three lowest eigenstates for several different values of Ω with $g_{\uparrow\downarrow} = 0.6g$. In Fig. 3(b), we plot ΔE_b, the energy difference between the two lowest energy states, as a function of Ω with several different values of $g_{\uparrow\downarrow}$. For now let us focus on the the case with $g_{\uparrow\downarrow} = 0.6g$ which is represented by the black solid line in Fig. 3(b). Depending on whether ΔE_b vanishes or not, the ground state then exhibits the following three phases as Ω varies:
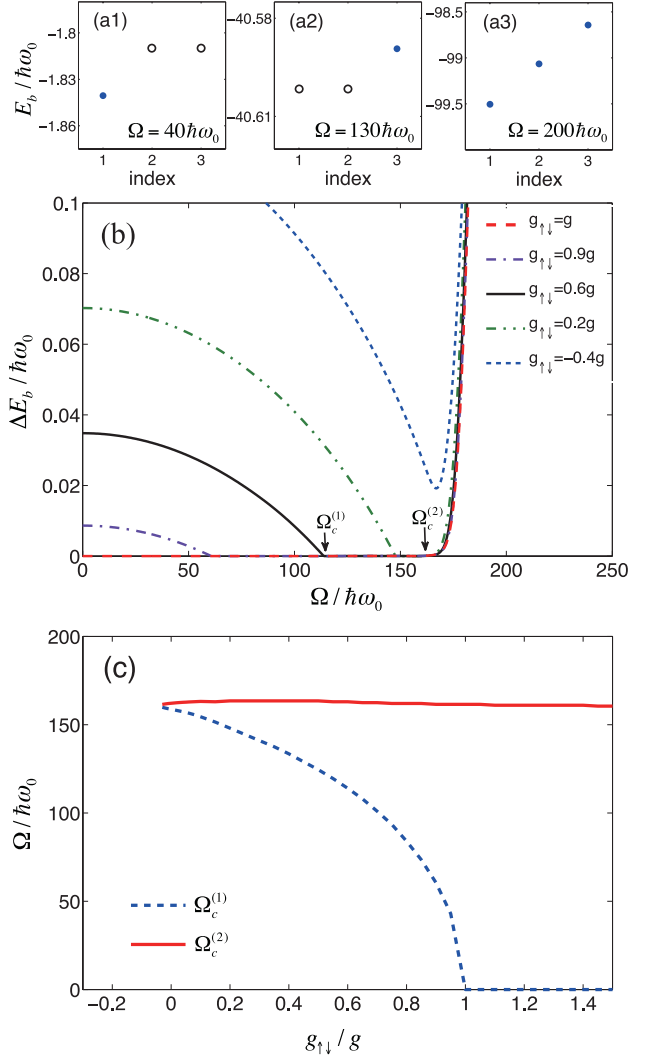

FIG. 3: (color online) (a) Energies of the lowest three two-boson eigenstates for $g_{\uparrow\downarrow}/g = 0.6$. Here solid and empty circles correspond to non-degenerate and degenerate states, respectively. (b) Energy difference between the two lowest energy states for the case of two weakly interacting bosons, as a function of Ω, for $g_{\uparrow\downarrow}/g = 1$, 0.9, 0.6, 0.2, -0.4. (c) $\Omega_c^{(1)}$ and $\Omega_c^{(2)}$ as functions of $g_{\uparrow\downarrow}$. The other parameters are: $\delta = 0$, $q_r = 10\sqrt{m\hbar\omega_0}$, $\omega = 2\omega_0$, $g = 0.16\hbar\omega_0$. The 1D interaction strength g is calculated from 3D interaction parameter $g_{3D} = 7.79 \times 10^{-12}$Hz cm^3 with a transverse trapping frequency $\omega_\perp = 100\omega_0$.

Phase I — When $\Omega < \Omega_c^{(1)} \approx 115\hbar\omega_0$, ΔE_b is finite, so the two-boson ground state is non-degenerate. In this regime, the single-particle ground state is two-fold degenerate and we label the two single-particle ground states as $|g_1\rangle$ and $|g_2\rangle$ (see discussion in Sec. II). The ground state of the two boson system can then be approximately represented as

$$|\Psi_g\rangle \approx |g_1 g_2\rangle_b \equiv \frac{1}{\sqrt{2}} \left(|g_1\rangle_1 |g_2\rangle_2 + |g_2\rangle_1 |g_1\rangle_2\right)\,. \quad (14)$$
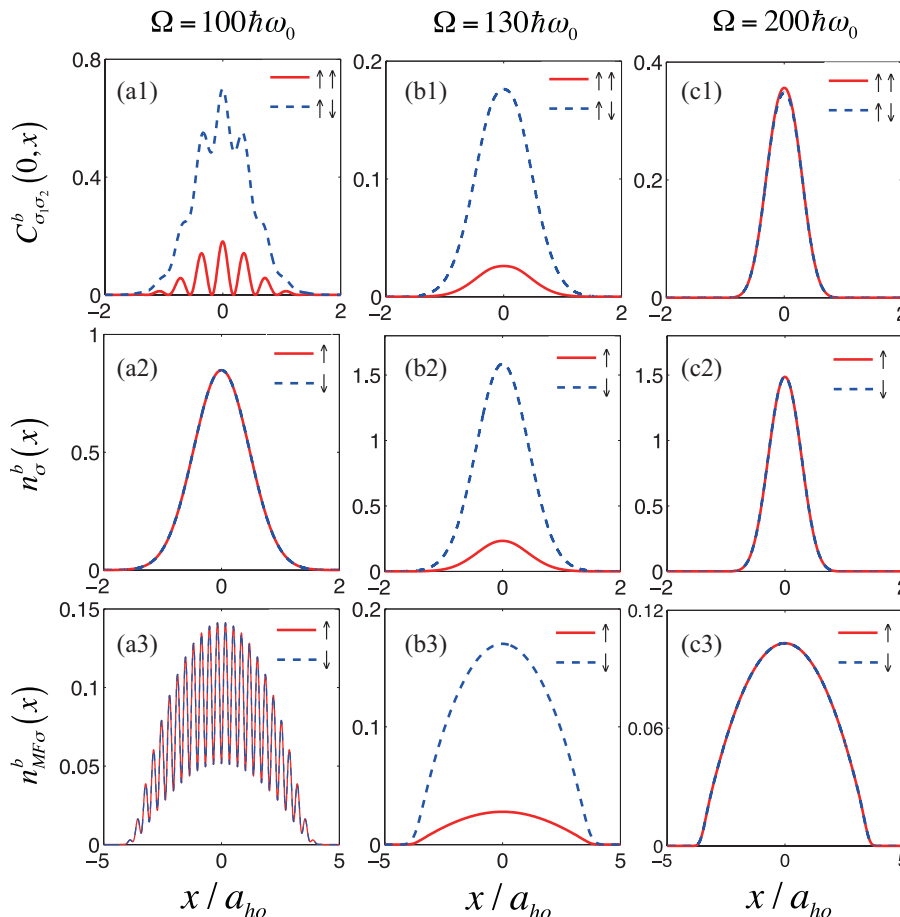
FIG. 4: (color online) (a1)-(c1) Density-density correlation functions of two-boson ground states. (a2)-(c2) Spin density profiles of two-boson ground states. (a3)-(c3) Mean-field ground state density profiles for a condensate of 1000 bosons. The figures are plotted for the cases with $\Omega/(\hbar\omega_0) = 100, 130, 200$, and $g_{\uparrow\downarrow} = 0.6g$, $\delta = 0$. At $\Omega = 130\hbar\omega_0$, the ground states are two-fold degenerate and the figures are for one of the degenerate states.

Hence the two bosons each occupies one of the single-particle ground states. Due to the bosonic statistics, the two bosons are highly entangled. In Fig. 4(a1) and (a2), we plot the density-density correlation $C_{\sigma_1\sigma_2}^b (0, x)$ and the spin density profiles $n_\sigma^b(x)$, respectively. The two-boson ground state features a smooth density profile identical for the two spin components. However, the entanglement manifests itself in the oscillations (or stripes) in $C_{\sigma_1\sigma_2}^b (0, x)$. Given the two-boson ground state in Eq. (14) and the single-particle ground states in Eqs. (6) and (7), we can explicitly write down the density-density correlation functions and spin density profiles as

$$C_{\uparrow\uparrow}^b(x_1, x_2) = C_{\downarrow\downarrow}^b(x_1, x_2) \approx A_1 + B\cos\left[2k\left(x_1 - x_2\right)\right];$$
$$C_{\uparrow\downarrow}^b(x_1, x_2) = C_{\downarrow\uparrow}^b(x_1, x_2) \approx A_2 + B\cos\left[2k\left(x_1 - x_2\right)\right],$$
$$n_\uparrow^b(x) = n_\downarrow^b(x) \approx \phi_1^2(x) + \phi_2^2(x), \tag{15}$$

with

$$A_1 \equiv \phi_1^2(x_1)\phi_2^2(x_2) + \phi_1^2(x_2)\phi_2^2(x_1); \tag{16}$$
$$A_2 \equiv \phi_1^2(x_1)\phi_1^2(x_2) + \phi_2^2(x_1)\phi_2^2(x_2);$$
$$B \equiv 2\phi_1(x_1)\phi_2(x_2)\phi_1(x_2)\phi_2(x_1).$$

being smooth functions of x_1 and x_2. The stripes in the density-density correlation arise from the sinusoidal terms in Eq. (15). We note in Fig. 3(a1) that in this phase, the first excited two-boson state is doubly degenerate. The two degenerate states roughly correspond to $|g_1 g_1\rangle_b$ and $|g_2 g_2\rangle_b$.

In order to connect the two-body physics to the many-body physics, we plot in Fig. 4(a3) the mean-field condensate density profile. The condensate wave function is obtained by minimizing the mean-field energy functional

$$E_{\mathrm{MF}} = \int dx \left[N\left(\Phi_\uparrow^* \ \Phi_\downarrow^*\right) h\left(\begin{array}{c} \Phi_\uparrow \\ \Phi_\downarrow \end{array}\right) \right. \tag{17}$$
$$\left. + \frac{N^2 g}{2}(|\Phi_\uparrow|^4 + |\Phi_\downarrow|^4) + N^2 g_{\uparrow\downarrow}|\Phi_\uparrow|^2|\Phi_\downarrow|^2 \right],$$

where $\Phi_\uparrow$ and $\Phi_\downarrow$ are the condensate wave functions of two spin components, and N is the total number of atoms, which we take to be 1000 in the calculation. Fig. 4(a3) shows that the condensate is in the so-called stripe phase where the density profile exhibits a stripe pattern. This stripe pattern can therefore be regarded as a manifestation of the stripes in the two-body correlation function shown in Fig. 4(a1), even though the two-body density profiles are smooth.
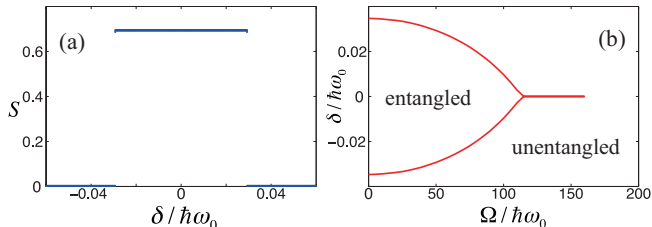

FIG. 5: (color online) (a) Von Neumann entanglement entropy of the two-boson ground state, as a function of δ. The figure is plotted for the case with $g_{\uparrow\downarrow} = 0.6g$ and $\Omega = 50\hbar\omega_0$. (b) The boundary of entangled and non-entangled ground states with $g_{\uparrow\downarrow} = 0.6g$, as a function of δ and Ω. In the "entangled" region , ground states are strongly entangled and thus exhibit stripes in density-density correlations. In the "unentangled" region, ground states are not entangled and show smooth density-density correlations. Other parameters: $q_r = 10\sqrt{m\hbar\omega_0}$, $\omega = 2\omega_0$, $g = 0.16\hbar\omega_0$.

Finally, let us consider the effect of finite two-photon detuning δ. A finite δ breaks the degeneracy of the single-particle ground state. Hence one may expect that for a large $|\delta|$, the ground state of the two weakly interacting bosons corresponds to an unentangled state with both bosons occupying the non-degenerate single-particle ground state. For this unentangled ground state, $C^b_{\sigma_1\sigma_2}(x_1, x_2)$ turns to be smooth. However, for a sufficiently small $|\delta|$, the two-boson ground state still roughly takes the form of Eq. (14), with $|g_1\rangle$, $|g_2\rangle$ representing the ground and first excited single-particle states, and thus $C^b_{\sigma_1\sigma_2}(x_1, x_2)$ still exhibits stripes. To demonstrate the variation of the entanglement, we plot in Fig. 5(a) the entanglement entropy S of the two-boson ground state, where $S = -\text{Tr}[\rho_1 \ln \rho_1]$ with $\rho_1 = \text{Tr}_2[|\Psi_g\rangle\langle\Psi_g|]$ being the reduced density matrix for particle 1. State represented by (14) is maximally entangled with $S = \ln 2$. Using the numerically obtained ground states with finite $|\delta|$, we find that S is very close to $\ln 2$ for $|\delta| < 0.03\hbar\omega_0$, and beyond this range, S quickly drops to 0, indicating an unentangled ground state. The range of δ within which the ground state is entangled is shown in Fig. 5(b) as a function of Ω. As Ω tends to $\Omega_c^{(1)}$, this range approaches zero. In Fig. 5(b), The "entangled" ("unentangled") region manifests itself in oscillating (smooth) density-density correlations.

Phase II — When $\Omega_c^{(1)} < \Omega < \Omega_c^{(2)}$, $\Delta E_b = 0$ indicates that the ground states have two-fold degeneracy.

Here $\Omega_c^{(2)} \approx 160\hbar\omega_0$ is very close to the critical Raman coupling strength Ω_c at which the single-particle ground state changes from degenerate to non-degenerate. Our result shows that the two degenerate two-boson ground states can be approximately represented as

$$|\Psi_{g1}\rangle \approx |g_1 g_1\rangle_b \equiv |g_1\rangle_1 |g_1\rangle_2 \,, \qquad (18)$$
$$|\Psi_{g2}\rangle \approx |g_2 g_2\rangle_b \equiv |g_2\rangle_1 |g_2\rangle_2 \,.$$

Hence the two bosons occupy the same single-particle ground state. In Fig. 4(b1) and (b2), we plot $C^b_{\sigma_1\sigma_2}(0, x)$ and $n^b_\sigma(x)$ for $|\Psi_{g1}\rangle$, respectively, whose explicit expressions in terms of the single-particle ground states are approximately given by:

$$
\begin{aligned}
C^b_{\uparrow\uparrow}(x_1, x_2) &\approx 2\phi_1^2(x_1)\phi_1^2(x_2) \,; &(19)\\
C^b_{\downarrow\downarrow}(x_1, x_2) &\approx 2\phi_2^2(x_1)\phi_2^2(x_2) \,;\\
C^b_{\uparrow\downarrow}(x_1, x_2) &\approx 2\phi_1^2(x_1)\phi_2^2(x_2) \,;\\
C^b_{\downarrow\uparrow}(x_1, x_2) &\approx 2\phi_1^2(x_2)\phi_2^2(x_1) \,,\\
n^b_\uparrow(x) &= 2\phi_1^2(x) \,;\\
n^b_\downarrow(x) &= 2\phi_2^2(x) \,.
\end{aligned}
$$

In this regime, both the density-density correlation functions and the spin density profiles are smooth functions of the position. In addition, the total magnetization $\mathbf{M} \equiv \int dx\, [n_\uparrow(x) - n_\downarrow(x)] \neq 0$ in this phase. The corresponding mean-field condensate density profiles are plotted in Fig. 4(b3). Here the condensate is in the so-called plane-wave phase and the density profiles for the two spin components are smooth. The condensate in this phase also exhibits the finite magnetization.

Note that the two degenerate states $|\Psi_{g1}\rangle$ and $|\Psi_{g2}\rangle$ represented in Eq. (18) are unentangled states. However, due to the degeneracy, any superposition state of $|\Psi_{g1}\rangle$ and $|\Psi_{g2}\rangle$ is still the ground state of the two-body system, and such a superposition state is entangled. However, this entanglement is not robust against a finite two-photon detuning δ: any finite δ will force both atoms to occupy the same non-degenerate single-particle ground state, and hence destroy the entanglement and result in the smooth $C^b_{\sigma_1\sigma_2}(x_1, x_2)$. This represents an essential difference for the ground state entanglement property between Phase I and II.

In Phase II, we note that the first excited state is non-degenerate as shown in Fig. 3(a2) and roughly corresponds to $|g_1 g_2\rangle_b$. Hence the ground state of Phase I corresponds to the first excited state of Phase II, and vice versa. These two phases result from the competition between the following two factors: (1) The quantum statistical property of bosons favors identical bosons to occupy the same single-particle state; and (2) the smaller interspecies interaction ($g_{\uparrow\downarrow} < g$) favors the bosons to occupy different spin states, and the smaller Raman coupling strength Ω induces more difference between the spins of $|g_1\rangle$ and $|g_2\rangle$.

Phase III — When $\Omega > \Omega_c^{(2)}$, the gap reopens as ΔE_b becomes finite again. In this regime, the single-particle ground state $|g\rangle$, whose wave function is given in Eq. (8), is also non-degenerate. The two-boson ground state can then be approximately represented by

$$|\Psi_g\rangle \approx |gg\rangle_b \equiv |g\rangle_1 |g\rangle_2 , \qquad (20)$$

which features a smooth $C_{\uparrow\uparrow}^b(0,x) \approx C_{\uparrow\downarrow}^b(0,x)$ and identical $n_\uparrow^b(x) = n_\downarrow^b(x)$, as shown in Fig. 4(c1) and (c2). The explicit expressions are approximately given by:

$$C_{\uparrow\uparrow}^b(x_1,x_2) = C_{\downarrow\downarrow}^b(x_1,x_2) \approx \tfrac{1}{2}\phi_0^2(x_1)\phi_0^2(x_2); \quad (21)$$
$$C_{\uparrow\downarrow}^b(x_1,x_2) = C_{\downarrow\uparrow}^b(x_1,x_2) \approx \tfrac{1}{2}\phi_0^2(x_1)\phi_0^2(x_2);$$
$$n_\uparrow^b(x) = n_\downarrow^b(x) \approx \phi_0^2(x).$$

The corresponding mean-field condensate density profiles are plotted in Fig. 4(c3). As in the two-body case, the condensate is smooth and features identical density profiles for the two spin components.

In this Phase, all the two-boson eigenstates are non-degenerate, as well as all the single-particle eigenstates. The weak interaction only causes small shifts of the eigenenergies, but does not affect the degeneracies.

B. Effects of $g_{\uparrow\downarrow}$ on two-body phase diagram

The above discussion demonstrates that, with $g_{\uparrow\downarrow} = 0.6g$, the ground state exhibits three phases separated by two critical Raman coupling strengths $\Omega_c^{(1)}$ and $\Omega_c^{(2)}$. Now let us discuss how the two-body phase diagram is changed when the inter-species interaction strength $g_{\uparrow\downarrow}$ is varied, while the intra-species interaction strength is fixed at value g.

In Fig. 3(a), we also plot the energy difference between the two lowest energy states for several other values of $g_{\uparrow\downarrow}$. The dependence of $\Omega_c^{(1)}$ and $\Omega_c^{(2)}$ on $g_{\uparrow\downarrow}$ are plotted in Fig. 3(b). From these plots, we see that $\Omega_c^{(1)}$ vanishes for $g_{\uparrow\downarrow} \geq g$. In other words, when the inter-species interaction strength exceeds the intra-species interaction strength, Phase I, and hence the stripe phase in the mean-field many-body regime, no longer exists. We have checked that this property is independent of the trap frequency ω.

As $g_{\uparrow\downarrow}$ decreases from g, $\Omega_c^{(1)}$ increases from zero and approaches $\Omega_c^{(2)}$, while $\Omega_c^{(2)}$ remains almost unchanged. Correspondingly, the parameter space where Phase II exists shrinks. At a critical value of $g_{\uparrow\downarrow}$, the two critical Raman coupling strengths merge, and for $g_{\uparrow\downarrow}$ smaller than this value, the two-body ground state is no longer degenerate for any values of Ω, and ΔE_b is always positive (see the curve in Fig. 3(a) with $g_{\uparrow\downarrow} = -0.4g$).

IV. TWO-FERMION GROUND STATE

The physics of the two-fermion ground state is quite different from that of two bosons, because of the antisymmetric nature and the Pauli exclusion principle for the quantum states of identical fermions. The Hamiltonian, the density-density correlation functions, and the spin density profiles of the two-fermion system are given by Eqs. (9), (12), and (13), respectively, where $|\Psi_g\rangle$ denotes the two-fermion ground state. As we are only considering s-wave contact interaction, there is no intra-species interaction between two fermions. To investigate the properties of this system, we expand the Hamiltonian onto the antisymmetric two-particle basis states $|ij\rangle_f \equiv \frac{1}{\sqrt{2}}(|i\rangle_1|j\rangle_2 - |j\rangle_1|i\rangle_2)$, and then follow a similar procedure as above for the two-boson case.
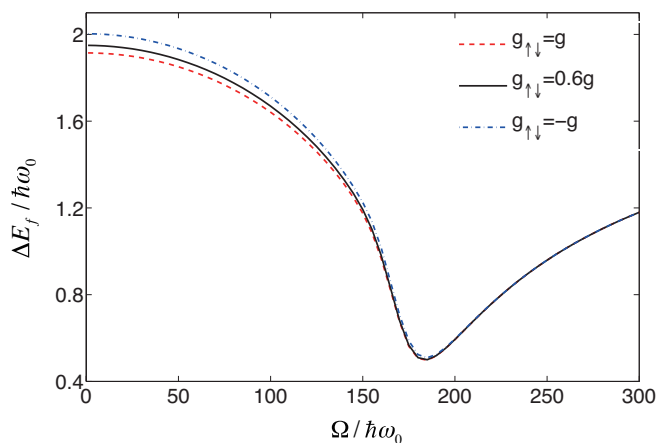

FIG. 6: (color online) For the case of two weakly interacting fermions, energy difference between the first excited state and the ground state, as a function of Ω with $g_{\uparrow\downarrow} = g, 0.6g, -g$. The parameters: $\delta = 0$, $q_r = 10\sqrt{m\hbar\omega_0}$, $\omega = 2\omega_0$, $\omega_\perp = 100\omega_0$, $g = 0.16\hbar\omega_0$.

Through exact diagonalization of the Hamiltonian in Eq. (9) with $\delta = 0$, we obtain ΔE_f, the energy difference between the two lowest-lying states, and plot it in Fig. 6 as a function of Ω for several different values of $g_{\uparrow\downarrow}$. As Ω increases from zero, ΔE_f first decreases and reaches a minimum near Ω_c (the critical value of the Raman coupling strength at which the single-particle ground state degeneracy is lifted), and then starts to increase again. The essential difference with the two-boson case is that here ΔE_f is always positive and never becomes zero. Furthermore, since in the weak interaction regime we are concerned, the interaction strength $g_{\uparrow\downarrow}$ does not have a significant effect on the system.

In Fig. 7, we display the properties of the two-fermion ground states for two Raman coupling strengths, one smaller and the other larger than Ω_c:

$\Omega < \Omega_c$ — For this case, the single-particle ground states, $|g_1\rangle$ and $|g_2\rangle$, are two-fold degenerate, and the
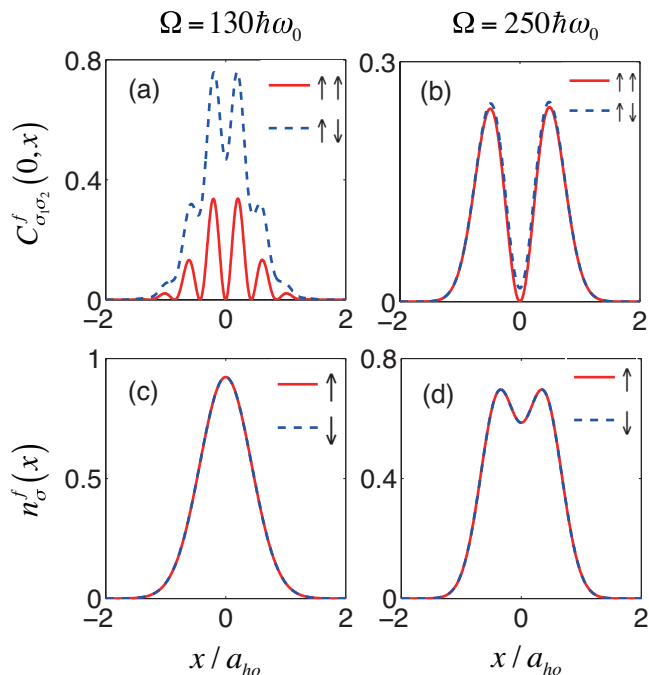
FIG. 7: (color online) (a)(b) Density-density correlations of two-fermion ground states, which satisfy $C_{\uparrow\uparrow}^f(0,x) = C_{\downarrow\downarrow}^f(0,x)$ and $C_{\uparrow\downarrow}^f(0,x) = C_{\downarrow\uparrow}^f(0,x)$. (c)(d) Spin density profiles of two-fermion ground states. The figures are plotted for the cases with $\Omega/\hbar\omega_0 = 130, 250$, $g_{\uparrow\downarrow} = 0.6g$ and $\delta = 0$.

two-fermion ground state can be approximately represented as

$$|\Psi_g\rangle \approx |g_1 g_2\rangle_f = \frac{1}{\sqrt{2}}\left(|g_1\rangle_1|g_2\rangle_2 - |g_2\rangle_1|g_1\rangle_2\right), \quad (22)$$

from which the correlation functions and density profiles can be straightforwardly calculated as

$$C_{\uparrow\uparrow}^f(x_1, x_2) = C_{\downarrow\downarrow}^f(x_1, x_2) \approx A_1 - B\cos\left[2k\left(x_1 - x_2\right)\right];$$
$$C_{\uparrow\downarrow}^f(x_1, x_2) = C_{\downarrow\uparrow}^f(x_1, x_2) \approx A_2 - B\cos\left[2k\left(x_1 - x_2\right)\right];$$
$$n_\uparrow^f(x) = n_\downarrow^f(x) \approx \phi_1^2(x) + \phi_2^2(x), \quad (23)$$

with A_1, A_2, and B given in Eq. (16). The numerical results are displayed in Fig. 7(a) and (c). For this case, the density-density correlation function $C_{\sigma_1\sigma_2}^f(x_1, x_2)$ is characterized by oscillations (or stripes) which arise from the sinusoidal terms in Eq. (23).

$\Omega > \Omega_c$ — For this case, the single-particle ground state $|g\rangle$ is non-degenerate. The two-fermion ground state can be approximately represented as

$$|\Psi_g\rangle \approx |ge\rangle_f = \frac{1}{\sqrt{2}}\left(|g\rangle_1|e\rangle_2 - |e\rangle_1|g\rangle_2\right), \quad (24)$$

where $|e\rangle$ denotes the non-degenerate single-particle first excited state. The density-density correlation functions and spin density profiles are displayed in Fig. 7(b) and

(d), respectively. In contrast to the single-peak structure in the previous case, here the spin density profile exhibits a double-peak structure because the real space probability profile of $|e\rangle$ features double peaks.

V. MEASURING THE INTERACTION INDUCED ENERGY GAP

In Sec. III, we have demonstrated that, for the two-boson case with $\delta = 0$, the energy gap ΔE_b in Phase I with $\Omega < \Omega_c^{(1)}$ is induced by the spin-dependent interaction. For fixed values of Ω and g in this regime, $g_{\uparrow\downarrow}$ and ΔE_b have a one-on-one mapping relation, and hence one can obtain the value of $g_{\uparrow\downarrow}$ through measuring ΔE_b.

In this section, we propose an experimental scheme to measure ΔE_b for the two-boson case. In the $\Omega < \Omega_c^{(1)}$ regime, we consider $|\Psi_g\rangle$ as an initial state perturbed by a harmonic trap with periodically modulated trapping frequency $\omega(t) = \omega\left[1 - \alpha\sin\left(\omega_v t\right)\right]$, where ω is the original trap frequency, ω_v is the modulation frequency, and $\alpha \ll 1$. The time evolution of the two-boson state $|\Psi(t)\rangle$ is then determined by the Schrödinger equation

$$i\hbar\frac{\partial}{\partial t}|\Psi(t)\rangle = H_v(t)|\Psi(t)\rangle, \quad (25)$$

where the time-dependent Hamiltonian

$$H_v(t) = h_1^v(t) + h_2^v(t) + \hat{V}, \quad (26)$$

where $h_i^v(t)$ take the form of Eq. (1) with ω replaced by $\omega(t)$. We study the time evolution of the system by solving Eq. (25) using the Crank-Nicolson method.

The measurement of ΔE_b can be conducted by making use of the resonant excitation of the system. We investigate how the periodic perturbations with various ω_v influence the probability $P_e(t)$ for the ground state being excited to the first excited state. In the following discussion, we consider $g_{\uparrow\downarrow} = 0.6g$ and $\Omega = 80\hbar\omega_0$, and hence define $\Delta E_b \equiv \Delta E_b(\Omega = 80\hbar\omega_0)$. For an on-resonance modulation with $\omega_v = \Delta E_b$, we see in Fig. 8(a) a significant growth of P_e, whereas for an off-resonance modulation with $\omega_v = 0.8\Delta E_b$, P_e never exceeds 0.5%. We plot in Fig. 8(b) the excitation probability P_e as a function of the modulation frequency ω_v at $\omega_0 t = 15000$, where a typical resonance peak is clearly seen.

In order to visualize the above resonant excitation process, we examine the time evolution of the total density profile which is defined as $n_b(x) \equiv n_\uparrow^b(x) + n_\downarrow^b(x)$. For the on-resonance case with $\omega_v = \Delta E_b$, $n_b(x)$ develops a stripe pattern as a function of t, as shown in Figs. 8(c1)-(c3). The presence of this stripe pattern is because $|\Psi(t)\rangle_b$ becomes a superposition of the ground state $|\Psi_g\rangle$ and the first excited state during the time evolution. However, for off-resonant modulation, the system is almost unaffected by the periodic perturbation, and the stripe pattern is not present in $n_b(x)$.
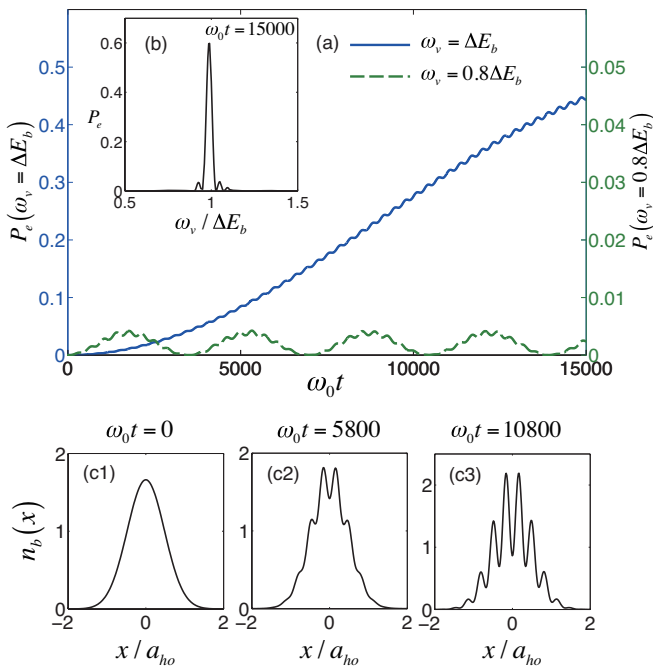
FIG. 8: (color online) Excitation of the two-boson ground state in a harmonic trap with periodically modulated trapping frequency $\omega\left[1 - \alpha \sin\left(\omega_v t\right)\right]$. We fix $g_{\uparrow\downarrow} = 0.6g$, $\Omega = 80\hbar\omega_0$, $\omega = 2\omega_0$, $\alpha = 0.05$, and choose the two-boson ground state as the initial state. (a) Probability $P_e\left(t\right)$ on the first excited state for the on-(off-)resonance case with $\omega_v = \Delta E_b\ (0.8\Delta E_b)$, as a function of time t. (b) P_e as a function of ω_v when $\omega_0 t = 15000$. (c1)-(c3) Time evolution of the total density profile $n_b\left(x\right)$ for the on-resonance case with $\omega_v = \Delta E_b$.

VI. CONCLUSION

In this paper we have systematically investigated the single-particle and two-body ground states of Raman-induced spin-orbit coupled ultracold atoms in a 1D harmonic trap. In the absence of the Raman coupling, all single-particle eigenstates are two-fold degenerate. As the Raman coupling strength increases, the degeneracy of higher energy eigenstates start to be lifted first, and eventually at a critical coupling strength, the ground state (and hence all energy eigenstates) becomes non-degenerate. The single-particle spectrum and wave functions help us to understand the two-body properties of the system for both bosons and fermions. For the two-boson case, we point out three phases distinguished by the behaviors of the degeneracy, density-density correlation functions, and spin density profiles. Then we identify a regime where the two atoms in the ground state are entangled and characterized by stripes in density-density correlations. This regime corresponds to the regime of the exotic stripe phase in the mean-field many-body limit. Our work therefore establishes a connection among one-, few- and many-body physics of trapped atomic systems with spin-orbit coupling.

[1] I. B. Spielman, Phys. Rev. A **79**, 063613 (2009).
[2] J. Dalibard, F. Gerbier, G. Juzeliūnas, and P. Öhberg, Rev. Mod. Phys. **83**, 1523 (2011).
[3] Y.-J. Lin, K. Jiménez-García, and I. B. Spielman, Nature **471**, 83-86 (2011).
[4] V. Galitski and I. B. Spielman, Nature **494**, 49-54 (2013).
[5] W. Zheng, Z.-Q. Yu, X. Cui, and H. Zhai, J. Phys. B: At. Mol. Opt. Phys. **46**, 134007 (2013).
[6] P. Wang, Z.-Q. Yu, Z. Fu, J. Miao, L. Huang, S. Chai, H. Zhai, and J. Zhang, Phys. Rev. Lett. **109**, 095301 (2012).
[7] L. W. Cheuk, A. T. Sommer, Z. Hadzibabic, T. Yefsah, W. S. Bakr, and M. W. Zwierlein, Phys. Rev. Lett. **109**, 095302 (2012).
[8] C. Wang, C. Gao, C.-M. Jian, and H. Zhai, Phys. Rev. Lett. **105**, 160403 (2010).
[9] T. D. Stanescu, B. Anderson, and V. Galitski, Phys. Rev. A **78**, 023616 (2008).
[10] H. Hu, H. Pu, J. Zhang, S.-G. Peng, and X.-J. Liu, Phys. Rev. A **86**, 053627 (2012).
[11] H. Hu, L. Jiang, X.-J. Liu, and H. Pu, Phys. Rev. Lett. **107**, 195304 (2011).
[12] Y. Li, L. P. Pitaevskii, and S. Stringari, Phys. Rev. Lett. **108**, 225301 (2012).
[13] G. I. Martone, Y. Li, and S. Stringari, Phys. Rev. A **90**, 041604(R) (2014).
[14] H. Zhai, Rep. Prog. Phys. **78**, 026001 (2015).
[15] L. Zhang, Y. Deng, and P. Zhang, Phys. Rev. A **87**, 053626 (2013).
[16] L. Dong, L. Jiang, H. Hu, and H. Pu, Phys. Rev. A **87**, 043616 (2013).
[16] H. Hu and S. Chen, arXiv:1302.5933 (2013).
[17] O. V. Marchukov, A. G. Volosniev, D. V. Fedorov, A. S. Jensen, and N. T. Zinner, J. Phys. B: At. Mol. Opt. Phys. **46**, 134012 (2013).
[18] B. M. Anderson and C. W. Clark, J. Phys. B: At. Mol. Opt. Phys. **46**, 134003 (2013).
[19] Q. Guan and D. Blume, Phys. Rev. A **92**, 023641 (2015).
[20] Q. Guan, X. Y. Yin, S. E. Gharashi and D. Blume, J. Phys. B: At. Mol. Opt. Phys. **47**, 161001 (2014).
[21] S. kar and R. R. Parwani, EPL, **80**, 30004 (2007).
[22] Yu. Kagan, E. L. Surkov, and G. V. Shlyapnikov, Phys. Rev. A **55**, R18(R) (1997).
[23] Y. Castin and R. Dum, Phys. Rev. Lett. **77**, 5315 (1996).